Redox Biology 24 (2019) 101207

Contents lists available at ScienceDirect

Redox Biology

journal homepage: www.elsevier.com/locate/redox

Quantification of carbonate radical formation by the bicarbonate-dependent peroxidase activity of superoxide dismutase 1 using pyrogallol red bleaching

Juan David Figueroa[a], Eduardo Fuentes-Lemus[a], Eva Dorta[a,b], Victoria Melin[c], Javiera Cortés-Ríos[d], Mario Faúndez[d], David Contreras[c], Ana Denicola[e], Beatriz Álvarez[f], Michael J. Davies[g], Camilo López-Alarcón[a,*]

[a] Departamento de Química Física, Facultad de Química y de Farmacia, Pontificia Universidad Católica de Chile, Chile
[b] Departamento de Nutrición y Ciencia de los Alimentos, Facultad de Farmacia, Universidad Complutense de Madrid, Madrid, Spain
[c] Laboratorio de Recursos Renovables, Facultad de Ciencias Químicas, Centro de Biotecnología, Universidad de Concepción.Chile
[d] Departamento de Farmacia, Facultad de Química y de Farmacia, Pontificia Universidad Católica de Chile, Chile
[e] Laboratorio de Fisicoquímica Biológica, Facultad de Ciencias, Universidad de la República, Uruguay
[f] Laboratorio de Enzimología, Facultad de Ciencias, Universidad de la República, Uruguay
[g] Department of Biomedical Sciences, Panum Institute, University of Copenhagen, Denmark

ARTICLE INFO

Keywords:
Carbonate radical anion
Superoxide dismutase
Hydrogen peroxide
Pyrogallol red
Peroxidase activity
Human SOD-1
Bovine SOD-1
EPR
DMPO
ABTS

ABSTRACT

Carbonate radicals ($CO_3^{\bullet -}$) are generated by the bicarbonate-dependent peroxidase activity of cytosolic superoxide dismutase (Cu,Zn-SOD, SOD-1). The present work explored the use of bleaching of pyrogallol red (PGR) dye to quantify the rate of $CO_3^{\bullet -}$ formation from bovine and human SOD-1 (bSOD-1 and hSOD-1, respectively). This approach was compared to previously reported methods using electron paramagnetic resonance spin trapping with DMPO, and the oxidation of ABTS (2,2-azino-bis(3-ethylbenzothiazoline)-6-sulfonic acid). The kinetics of PGR consumption elicited by $CO_3^{\bullet -}$ was followed by visible spectrophotometry. Solutions containing PGR (5–200 μM), SOD-1 (0.3–3 μM), H_2O_2 (2 mM) in bicarbonate buffer (200 mM, pH 7.4) showed a rapid loss of the PGR absorption band centered at 540 nm. The initial consumption rate (R_i) gave values independent of the initial PGR concentration allowing an estimate to be made of the rate of $CO_3^{\bullet -}$ release of 24.6 ± 4.3 μM min^{-1} for 3 μM bSOD-1. Both bSOD-1 and hSOD-1 showed a similar peroxidase activity, with enzymatic inactivation occurring over a period of 20 min. The single Trp residue (Trp^{32}) present in hSOD-1 was rapidly consumed (initial consumption rate 1.2 ± 0.1 μM min^{-1}) with this occurring more rapidly than hSOD-1 inactivation, suggesting that these processes are not directly related. Added free Trp was rapidly oxidized in competition with PGR. These data indicate that PGR reacts rapidly and efficiently with $CO_3^{\bullet -}$ resulting from the peroxidase activity of SOD-1, and that PGR-bleaching is a simple, fast and cheap method to quantify $CO_3^{\bullet -}$ release from bSOD-1 and hSOD-1 peroxidase activity.

1. Introduction

Superoxide radical anions, $O_2^{\bullet -}$, are generated in biological systems by several mechanisms including electron leakage from the mitochondrial electron transport chain, by a number of enzymes (e.g. the NADPH oxidase family, xanthine oxidase, uncoupled nitric oxide synthases), by autoxidation of a wide range of endogenous compounds (e.g. catechols, thiols), redox cycling of exogenous compounds (e.g. quinones, paraquat), and by autoxidation of metal ion-O_2 complexes (e.g. oxyhemoglobin and oxymyoglobin) [1]. The major fate of $O_2^{\bullet -}$ is dismutation to generate hydrogen peroxide (H_2O_2) and O_2, which can occur either spontaneously or catalyzed by the enzyme superoxide dismutase (SOD) (reaction (1)).

$$2\ O_2^{\bullet -} + 2H^+ \xrightarrow{SOD} H_2O_2 + O_2 \quad (1)$$

Under physiological conditions, the H_2O_2 produced via reaction (1) is rapidly removed by enzymes including catalase, peroxiredoxins, and glutathione peroxidases [1]. Thus, SOD and these enzyme families work in a coordinated manner to maintain the redox status of cells and biological fluids, inhibiting (or delaying) the damage triggered by reactive oxygen species (ROS) [1]. Nonetheless, in environments with high H_2O_2 concentrations, such as inflammatory conditions or inside peroxisomes, the cytosolic isoform of SOD (Cu,Zn-SOD, SOD-1) displays a bicarbonate- or CO_2– dependent peroxidase activity [2–7]. The

* Corresponding author.
E-mail address: clopezr@uc.cl (C. López-Alarcón).

https://doi.org/10.1016/j.redox.2019.101207
Received 26 February 2019; Received in revised form 17 April 2019; Accepted 23 April 2019
Available online 27 April 2019

chemical mechanism is still controversial, however, it is known that H_2O_2 reacts with the catalytic copper ion (Cu^{2+}) of SOD-1 generating a copper-bound oxidant. This is proposed to oxidize bicarbonate (HCO_3^-) to give the carbonate radical anion ($CO_3^{\bullet-}$) [8], or react with His residues of the protein ($CO_3^{\bullet-}$ also can react with His) to inactivate the enzyme [7,9].

$CO_3^{\bullet-}$ is a powerful oxidant ($E^{0'}_{red}$ = 1.78 V) and a highly reactive species [3], which is able to diffuse away from the catalytic site of SOD-1 to induce oxidation of surrounding molecules. A significant target appears to be the single tryptophan (Trp^{32}) residue of human SOD-1 (hSOD-1) [3,10], and it has been reported that $CO_3^{\bullet-}$-mediated oxidation of this residue to Trp-derived indolyl radicals is involved in the covalent dimerization (and oligomerization) of hSOD-1 through the formation of covalent Trp-Trp dimers [10]. This process may be of pathological relevance as $CO_3^{\bullet-}$ induced unfolding, oligomerization, and nonamyloid aggregation of hSOD-1 has been suggested as a contributing factor in triggering familial amyotrophic lateral sclerosis (ALS, also known as motor neurone disease, MND, or Lou Gehrig's disease) [11]. The formation of Trp-Trp cross-links in hSOD-1 dimers, or between different proteins or peptides, have been proposed as a marker of $CO_3^{\bullet-}$ formation in biological systems [12–14]. Tyr residues, which are not present in hSOD-1, are also prone to oxidation by $CO_3^{\bullet-}$ to the corresponding phenoxyl radicals [15,16]. Further reaction of these radicals results in the formation of Tyr-Tyr or Tyr-Trp bonds and cross-linking of protein disulfide isomerase [17].

Further studies have demonstrated that $CO_3^{\bullet-}$ can be formed via multiple other pathways, including Fenton reactions in the presence of bicarbonate buffers [18], by pulsed laser light [19], in photochemical reactions employing Co(III) carbonate complexes [14,20], in xanthine oxidase turnover [21], via radiolysis [22–24], and in peroxynitrite-mediated processes in the presence of CO_2 [4,13,25–28]. These data together with information on the powerful oxidizing capacity and high reactivity of this species, have stimulated further studies on the physiopathological significance of $CO_3^{\bullet-}$ formation.

In the context of SOD-1-mediated generation of $CO_3^{\bullet-}$ through its peroxidase activity, determination of the rate of $CO_3^{\bullet-}$ production is of particular value and importance. A number of oxidizable probes have been employed in this regard, together with spectroscopic techniques. Thus, $CO_3^{\bullet-}$-mediated oxidation of dichloro-dihydro-fluorescein to dichloro-fluorescein [29,30], dihydrorhodamine 123 to rhodamine [30,31], and ABTS (2,2-azino-bis(3-ethylbenzothiazoline)-6-sulfonic acid) to $ABTS^{\bullet+}$ [7,32] have been examined. Electron paramagnetic resonance (EPR) with spin trapping has also been used to estimate the yield of $CO_3^{\bullet-}$ formation from the SOD-1-related peroxidase activity [14,21,33]. In the presence of the spin trap DMPO (5,5-dimethyl-1-pyrroline *N*-oxide), $CO_3^{\bullet-}$ generates a spin adduct with a 1:2:2:1 hyperfine coupling pattern identical to that formed by the hydroxyl radical, $HO^{\bullet}$, and assigned to DMPO-OH. The formation of this species has been rationalized in terms of one-electron oxidation of the spin trap and subsequent reaction with water to give the hydroxyl adduct, DMPO-OH [33].

In spite of the considerable interest in the production and biochemical implications of $CO_3^{\bullet-}$, few data have been reported regarding the quantification of $CO_3^{\bullet-}$ production by SOD-1 in the presence of H_2O_2 and bicarbonate (HCO_3^-). In the light of our knowledge and experience using pyrogallol red (PGR, pyrogallolsulfonephthalein) as a probe to assess the generation of other oxidants [34–38], we hypothesized that $CO_3^{\bullet-}$-mediated bleaching of the optical absorbance band of PGR at ~540 nm might allow quantification of $CO_3^{\bullet-}$ formation by SOD-1/H_2O_2/HCO_3^- systems. Furthermore, the kinetic profiles of PGR consumption would allow to estimate the rate of $CO_3^{\bullet-}$ release, through a simple, fast and cheap methodology. This assay is a rapid and convenient way to quantify (or standardize) production of $CO_3^{\bullet-}$ through the peroxidase activity of SOD-1, and may be an effective tool to examine the chemistry of protein oxidation/crosslinking mediated by the SOD-1/H_2O_2/HCO_3^- system.

2. Materials and Methods

2.1. Materials

Superoxide dismutase from bovine erythrocytes (bSOD-1) was obtained from Sigma Aldrich (St Louis, MO, USA) whilst the recombinant wild-type human Cu, Zn superoxide dismutase (hSOD-1) was expressed in *E. coli* and purified by ammonium sulfate fractionation, ion exchange chromatography and gel filtration as described by Álvarez et al. [39]. 2,2′-Azino-bis(3-ethylbenzothiazoline-6-sulfonic acid) diammonium salt (ABTS), 5,5-dimethyl-1-pyrroline *N*-oxide (DMPO), pyrogallol red (PGR), diethylenetriaminepenta acetic acid (DTPA), manganese (IV) oxide (MnO_2), and L-tryptophan were purchased from Sigma Aldrich (St. Louis, MO, USA). Dimethylsulfoxide (DMSO), hydrogen peroxide (H_2O_2) and isopropanol were obtained from Merck KGaA (Darmstadt, Germany). All buffers and solutions were prepared with ultrapure water.

2.2. Production and detection of $CO_3^{\bullet-}$

$CO_3^{\bullet-}$ was generated via the peroxidase activity of bSOD-1 or hSOD-1 (0.3–30 μM per dimer) in the presence of H_2O_2 (1–10 mM) and DTPA (0.1 mM) in freshly-prepared HCO_3^- buffer (200 mM) adjusted with CO_2 to pH 7.4.

2.2.1. Detection of $CO_3^{\bullet-}$ by EPR

$CO_3^{\bullet-}$ was detected by EPR spin trapping using DMPO (50 mM) [14,33]. Samples containing bSOD-1, H_2O_2 and DTPA, in HCO_3^- (200 mM, pH 7.4) or phosphate buffer (75 mM, pH 7.4) were transferred into a BRAND capillary. Then, were sealed and introduced in the EPR cavity inside of an EPR sample tube (ER 221TUB/, 4 mm I.D.). The EPR spectra were recorded at 18 °C at X-band frequencies (~9 GHz) using a Bruker EMX instrument. The concentration of the DMPO-OH spin adduct (in arbitrary units) was measured as the intensity of the peaks as no variation in the line width was apparent. The potential role of $HO^{\bullet}$ in the formation of DMPO-OH was examined in control experiments carried out in the presence of DMSO (5 mM) or isopropanol (5 mM) with which $HO^{\bullet}$ reacts at near diffusion controlled rates ($k \sim 10^9$ $M^{-1}\,s^{-1}$) [1].

2.2.2. Oxidation of ABTS elicited by $CO_3^{\bullet-}$

Formation of $ABTS^{\bullet+}$ from ABTS induced by the SOD-1/H_2O_2/HCO_3^-system was followed by UV–visible spectrophotometry and EPR. Solutions containing ABTS (30 or 100 μM), bSOD-1 (3 μM per dimer), H_2O_2 (2 mM), and DTPA (0.1 mM) were incubated in HCO_3^- buffer (200 mM, pH 7.4). These solutions were placed in a thermostated cell of an Agilent 8453 spectrophotometer, and kinetics were followed at 740 nm. For EPR analysis, $ABTS^{\bullet+}$ was also generated using MnO_2, with solutions of ABTS (100 μM) and MnO_2 (25 mg mL^{-1}) in phosphate buffer (75 mM, pH 7.4) and DTPA (0.1 mM) incubated for 3 min. Excess MnO_2 was then removed by filtration using 0.2 μm filters (Merck, Millex-FG; 0,20 μm), and solutions transferred via syringe to a capillary Aqua X cell in a Bruker 4108 TMH/9701 instrument. EPR spectra were recorded as described above.

2.3. Consumption of PGR by $CO_3^{\bullet-}$

PGR solutions (15–200 μM) were prepared in HCO_3^- buffer (200 mM, pH 7.4) and incubated with bSOD-1 or hSOD-1 (0.3–30 μM per dimer), H_2O_2 (1–10 mM), and DTPA (0.1 mM). PGR consumption was followed spectrophotometrically by measuring the absorbance decrease at wavelengths between 540 and 590 nm, employing an Agilent 8453 spectrophotometer. Slopes at t = 0 min of normalized absorbance (A/A_0) versus time plots were obtained using the best fitting curve, and employing to determine initial consumption rates of PGR (initial slope of kinetic profiles multiplied by initial PGR concentration).

2.4. Monitoring intrinsic fluorescence changes of hSOD-1 and free Trp elicited by $CO_3^{\bullet -}$

Solutions containing each SOD-1 (3 μM per dimer), H_2O_2 (2 mM) and DTPA (0.1 mM) in HCO_3^- buffer (200 mM) adjusted at pH 7.4, were incubated at 37 °C in a quartz cuvette placed in the holder of a LS-55 PerkinElmer fluorimeter. The intrinsic fluorescence of hSOD-1, associated with its single Trp residue, was followed at 360 nm (using λ_{ex} 295 nm). Oxidation of free Trp (6 μM), induced by the mixture of bSOD-1 (3 μM as dimer), H_2O_2 (2 mM) and DTPA (0.1 mM) in HCO_3^- buffer was followed employing the same wavelengths of hSOD-1.

2.5. Data and statistical analysis

Results were obtained from experiments carried out in triplicate from at least three independent experiments. Data are presented as means ± SD. Data were considered to be statistically different from controls when $p < 0.05$, as determined by one-way ANOVA with Tukey's post-hoc test (carried out using Origin 8.0).

3. Results

3.1. EPR and UV–visible studies of $CO_3^{\bullet -}$ formation by HCO_3^--dependent bSOD-1 peroxidase activity

Fig. 1 shows EPR spectra obtained after 3 min incubation of bSOD-1 (0.3–30 μM) and H_2O_2 (2 mM) in HCO_3^- buffer containing DTPA (0.1 mM) and DMPO (50 mM). In agreement with previous reports [21,33], a quartet signal with intensity ratios of 1:2:2:1 was detected with hyperfine coupling constants $a_N = a_H = 1.49$ mT. This signal is assigned to the DMPO-OH spin adduct arising from $CO_3^{\bullet -}$-mediated oxidation of the spin trap to give the DMPO radical-cation and subsequent reaction with H_2O [4]. Low intensity triplet species were also registered in some spectra, which could be associated with secondary products derived form DMPO-OH [40]. Control incubations containing all the reagents with the exception of bSOD-1 (Fig. 1, spectrum d), or with the enzyme but using phosphate buffer (75 mM, pH 7.4, spectrum e in Fig. 1) with DTPA 0.1 mM, did not yield this adduct species. With the complete incubation system and HCO_3^- buffer, the inclusion of isopropanol or DMSO at 5 mM did not modulate the intensity of the observed signal in a significant manner, discounting a role for $HO^{\bullet}$ in the generation of this species (data not shown). The intensity of the DMPO-OH signal did not show a direct linear relationship with bSOD-1 concentration; with 3 μM bSOD-1 the spectral intensity (which is directly proportional to the radical concentration) was 3.5- and 1.5-fold higher than that detected with 0.3 and 30 μM bSOD-1 respectively (Fig. 1). The observed bell shaped concentration dependence is believed to arise from the difference in the rate of spin trap oxidation to DMPO-OH, induced by $CO_3^{\bullet -}$, and a rapid SOD-1-dependent decay of the spin adduct (data not shown). The latter may reflect over-oxidation of DMPO-OH by $CO_3^{\bullet -}$ or a SOD-bound intermediate, with a consequent loss of the spin adduct signal. These data clearly indicate limitations in the use of the EPR spin trapping method for quantifying $CO_3^{\bullet -}$ generation.

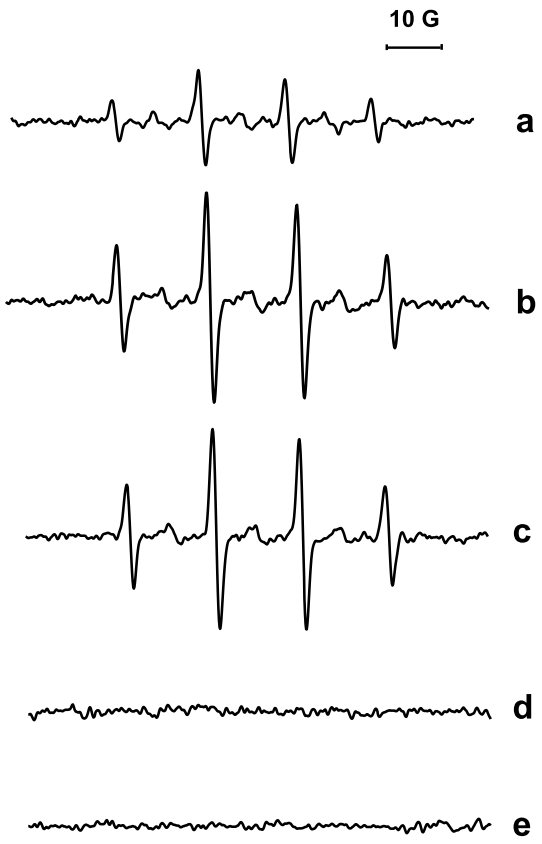

Fig. 1. Formation of $CO_3^{\bullet -}$ from the peroxidase activity of bSOD-1 assessed by EPR employing DMPO as spin trap. Solutions, in bicarbonate buffer (200 mM, pH 7.4), with or without bSOD-1, H_2O_2 (2 mM), DTPA (0.1 mM) and DMPO (50 mM) were incubated in the EPR cell at 20 °C. a–c: EPR spectra registered after 3 min incubation of solutions containing bSOD-1 at 0.3, 3 and 30 μM (as dimer), respectively. d: EPR spectrum obtained in the absence of bSOD-1. e: EPR spectrum obtained in the presence of bSOD-1 (3 μM), but incubated in phosphate buffer (75 mM, pH 7.4) with DTPA (0.1 mM). Representative data from n = 3 independent experiments.

Oxidation of ABTS to the corresponding radical cation ($ABTS^{\bullet +}$) has been employed previously to examine $CO_3^{\bullet -}$ formation by SOD-1 peroxidase activity [5]. The generation of $ABTS^{\bullet +}$ was followed by both EPR and UV–visible spectrophotometry. Incubation of ABTS with the bSOD-1/H_2O_2 system in HCO_3^- buffer containing DTPA 0.1 mM, as described above, gave rise to a weak EPR signal (black spectrum, Fig. 2A) assigned to $ABTS^{\bullet +}$. The assignment of this signal to $ABTS^{\bullet +}$, was confirmed by experiments employing MnO_2 as the oxidant [41], with this reaction system yielding a strong, well-defined, spectrum from $ABTS^{\bullet +}$ (red spectrum, Fig. 2A). Formation of $ABTS^{\bullet +}$ by the bSOD-1/H_2O_2/HCO_3^- system was also confirmed by visible spectrophotometry. As shown in Fig. 2B, incubation of ABTS with bSOD-1/H_2O_2 in HCO_3^- buffer containing DTPA 0.1 mM, lead to the formation of the characteristic spectrum of $ABTS^{\bullet +}$ with well-defined absorbance bands at ~405 nm and in the region 600–850 nm, with a maximum at 740 nm characteristic of this species [42]. Time course studies on the intensity of the absorbance band at 740 nm (Fig. 2C) showed that a maximum intensity (~0.2 AU) was reached after 9 min incubation, followed by a clear diminution over time, with this decreasing to ~ 0.07 AU at 83 min. This biphasic dependence clearly limits the use of ABTS oxidation as a tool to quantify $CO_3^{\bullet -}$ formation.

3.2. Bleaching of PGR induced by $CO_3^{\bullet -}$ generated from HCO_3^- dependent bSOD-1 peroxidase activity

Fig. 3A shows the changes in the optical absorbance spectrum of PGR elicited by incubation of PGR (60 μM) with bSOD-1/H_2O_2 in HCO_3^- buffer containing 0.1 mM DTPA. A decrease at 540 nm was observed together with formation of a new band at 395 nm. Control experiments in the absence of H_2O_2 (data not shown) showed that the presence of bSOD-1 did not alter the absorbance spectrum of PGR, consistent with the lack of a strong binding of the dye to the protein. Thus the changes in PGR absorbance are attributed to oxidation of free PGR. Direct molecular oxidation of PGR by H_2O_2 appears not to be a major contributor, as incubation of PGR with varying concentrations of H_2O_2 (2–10 mM) in HCO_3^- buffer with 0.1 mM DTPA, but no bSOD-1, gave only minor changes in absorbance (data not shown) when compared to the complete system.

The kinetics of $CO_3^{\bullet -}$-mediated bleaching of PGR was examined at

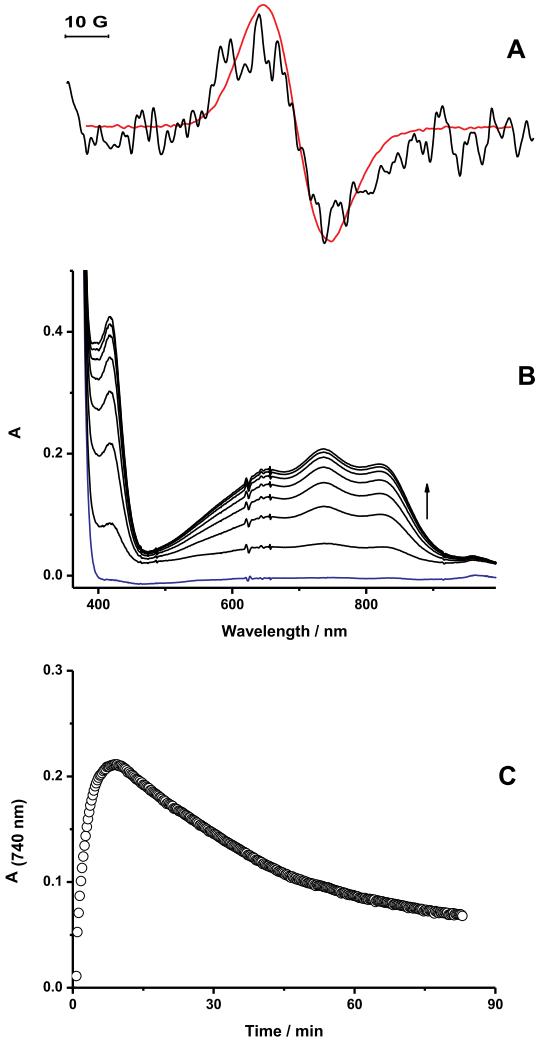

Fig. 2. Oxidation of ABTS to ABTS$^{\cdot+}$ by $CO_3^{\cdot-}$ derived from the peroxidase activity of bSOD-1. Panel A: EPR spectra obtained after 3 min incubation of solutions containing either ABTS 100 μM and MnO_2 (25 mg L^{-1}), red line, or ABTS (30 μM), bSOD-1 (3 μM), H_2O_2 (2 mM), and DTPA (0.1 mM), black line. Originally, the latter signal (black spectrum) had a gain 30 times lower than the red EPR signal. To compare both results, signals were normalized. Panel B: UV–visible spectra recorded during the incubation of ABTS (30 μM) and a bSOD-1 (3 μM)/H_2O_2 (2 mM) system in bicarbonate buffer (200 mM, pH 7.4, DTPA 0.1 mM). Blue line; spectrum registered at zero incubation time. The plot shows the spectra over the time period 0–9 min, the arrow indicates the progressive increase of the sample absorbance. Panel C: Kinetic profile of ABTS$^{\cdot+}$ formation followed at 740 nm. Representative data from n = 3 independent experiments.

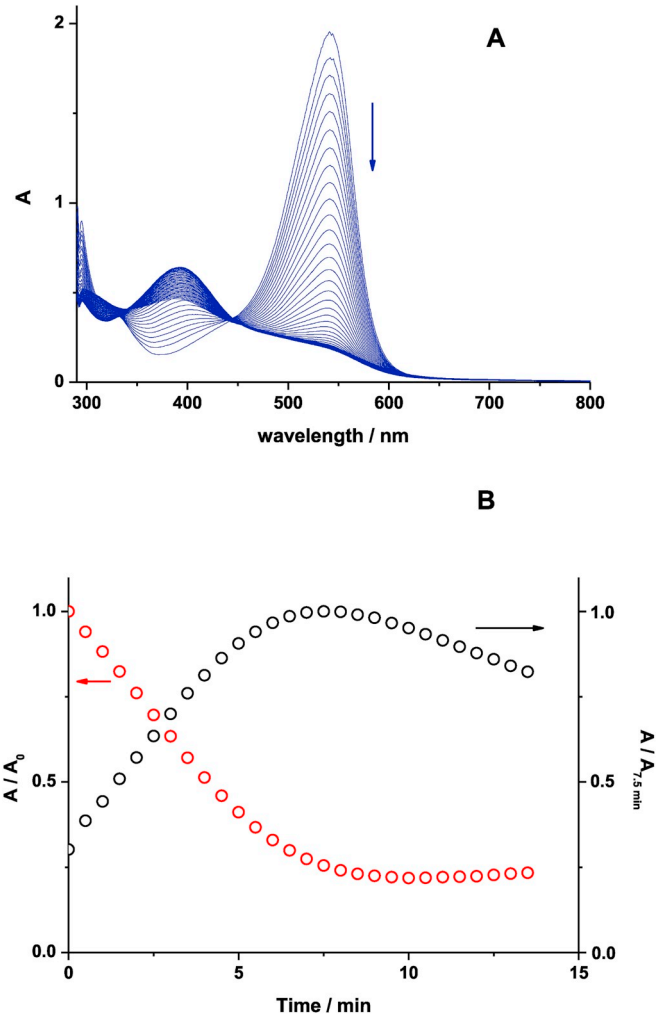

Fig. 3. Bleaching of PGR induced by $CO_3^{\cdot-}$. Solutions of PGR (60 μM) in bicarbonate buffer (200 mM, pH 7.4) and DTPA (0.1 mM) were incubated in the presence of bSOD-1 (3 μM) and H_2O_2 (2 mM). Panel A: changes in the UV–visible spectrum of PGR recorded during the incubation, the arrow indicates the decrease of the absorbance intensity in the 500–600 nm region. As the absorbance value at 540 nm was higher than 1.0, kinetic profiles for these samples were followed at longer wavelengths (usually 570–590 nm). Panel B: Kinetic profiles of PGR bleaching followed at 580 nm (red circles), and oxidized product(s) followed at 395 nm (black circles). Data at 395 were normalized with absorbance at 7.5 min (maximum intensity). Representative data from n = 3 independent experiments.

wavelengths between 540 and 590 nm depending on the PGR concentration employed, with the wavelength chosen to keep the maximum absorbance below 1 AU (the upper limit for linear absorbance responses on most spectrophotometers). These experiments showed a fast decrease in absorbance over the range 540–590 nm (see, for example, Fig. 3B for data obtained at 580 nm) together with a concomitant matching increase in absorbance at 395 nm. The latter increase in absorbance showed a small diminution at long time points after complete consumption of parent PGR (Fig. 3B), consistent with further modification of the product formed from PGR. However the initial rates of change in absorbance for both bands are not significantly different and, in the first minutes of reaction, a good isobestic point was detected at ~440 nm consistent with stoichiometric conversion of PGR to a single product. This behavior was observed only in the presence of HCO_3^-, as reactions carried out in phosphate buffer (75 mM, pH 7.4) with DTPA 0.1 mM gave rise to negligible (with 0.3 μM bSOD-1), or very limited (with 3 μM bSOD-1) absorbance changes (Supplementary Figs. 1A and B, respectively), indicating that PGR bleaching is directly associated with $CO_3^{\cdot-}$ production. Addition of HCO_3^- (1 mM) to phosphate-buffered solutions containing PGR/bSOD-1/H_2O_2 restored the bleaching activity (Supplementary Fig. 1B).

In HCO_3^- buffer, the bSOD-1/H_2O_2 mixture induced PGR bleaching with a linear initial dependence of the consumption rate (R_i, in μM min^{-1}) with increasing bSOD-1 concentration, described by the expression y = 0.113 + 5.0x, with r^2 = 0.998 (Fig. 4). Thus each micromolar of bSOD-1 added to the reaction solutions increased the R_i value (in μM min^{-1}) by 5-fold. On the other hand, with a fixed concentration of bSOD-1 of 0.3 μM, the R_i values were independent of the initial PGR concentration over the range 5–200 μM (Fig. 5). With a 10-fold higher concentration of bSOD-1 (i.e. 3 μM), an increase in R_i with increasing PGR concentration was observed over the range 5–30 μM. However with PGR concentrations > 30 μM, the R_i values were

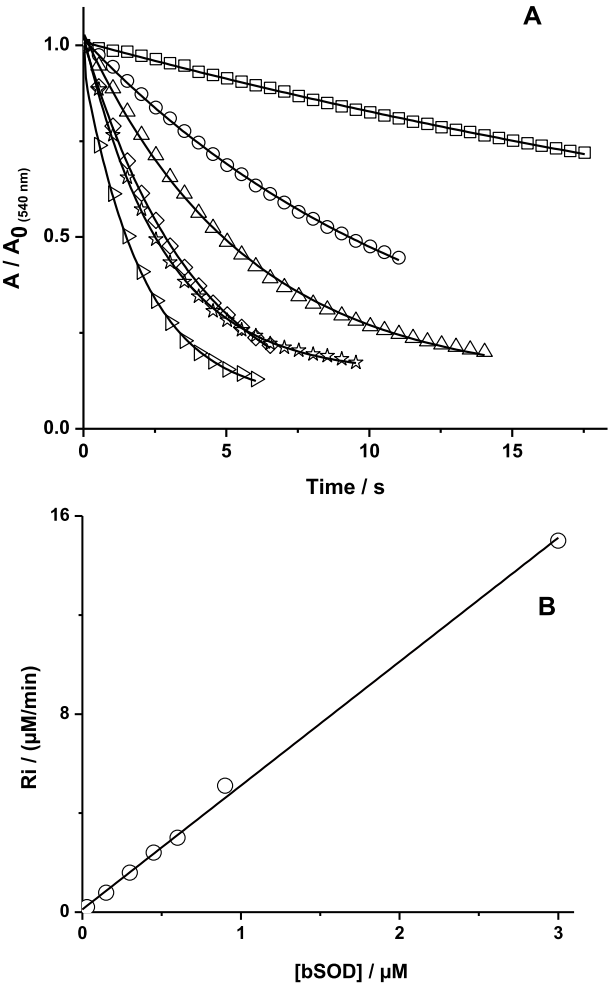

Fig. 4. Time course (panel A) and initial consumption rates (R_i, panel B) of PGR (15 μM) oxidation as consequence of its incubation with different concentrations of bSOD□0.03 μM; ○ 0.15 μM; △ 0.3 μM; ◇ 0.45 μM; ☆ 0.6 μM; ▷ 0.9 μM) in bicarbonate buffer solution (200 mM, pH 7.4) with DTPA (0.1 mM).

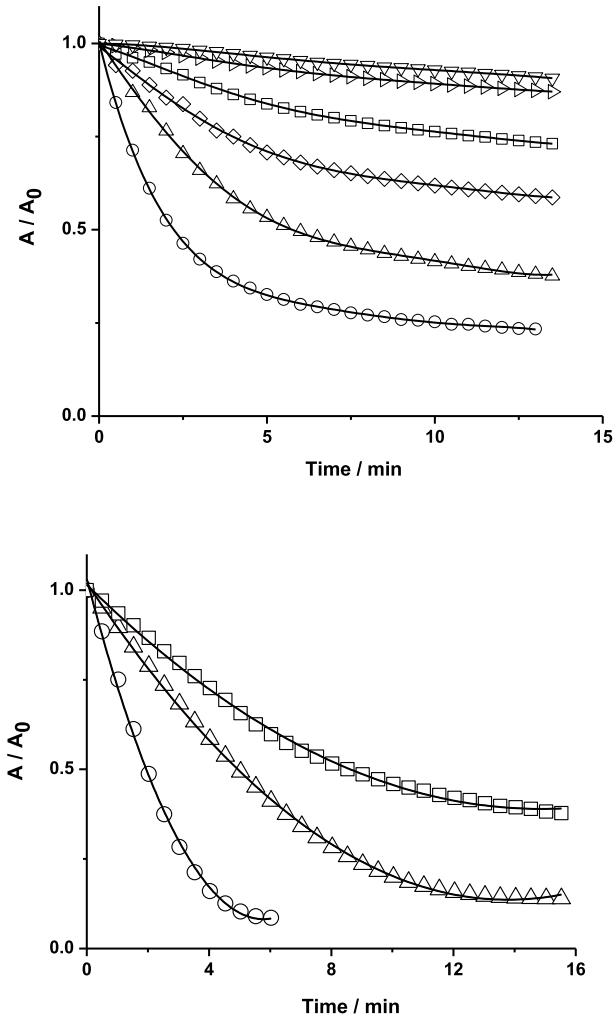

Fig. 5. Kinetic profiles of PGR consumption elicited by $CO_3^{\bullet-}$ at different PGR concentrations. Solutions were incubated in bicarbonate buffer (200 mM, pH 7.4) in the presence of H_2O_2 (2 mM), DTPA (0.1 mM), and 0.3 (panel A) or 3 (panel B) μM bSOD-1. Panel A: [PGR] = 5 (○), 15 (△), 30 (◇), 40□, 100 (▷), and 200 (▽) μM. Panel B: [PGR] = 15 (○), 60 (△), and 200 (□) μM. Depending on the PGR concentration, the kinetics were followed at wavelengths between 540 and 590 nm. Representative data from n = 3 independent experiments.

independent of the initial PGR concentration and reached a mean value of 12.3 ± 2.1 μM min^{-1} (Fig. 6). These data indicate that as long as the PGR concentration is significantly high over the SOD concentration (by ~10-fold) the R_i values are not dependent on PGR concentration, therefore could be considered as accurate indicators of the rate of $CO_3^{\bullet-}$ production.

As the bovine and the human isoform of SOD-1 show marked sequence identity and similarity, PGR consumption induced by $CO_3^{\bullet-}$ was also examined with the human isoform. Control experiments indicated that, as with bSOD-1, the hSOD-1 did not alter the UV–visible spectrum of PGR. Under identical experimental conditions with complete oxidation systems containing 3 μM SOD-1, H_2O_2 2 mM, and 30 μM PGR, the kinetic profiles for PGR bleaching gave statistically-identical ($p = 0.3535$) R_i values of 10.9 ± 1.9 and 9.6 ± 1.0 μM min^{-1} for bSOD-1 and hSOD-1, respectively.

To test if the rate of $CO_3^{\bullet-}$ generation was constant from bSOD-1 or hSOD-1, after total PGR bleaching, new aliquots of PGR were added to the incubations. If the generation rate of $CO_3^{\bullet-}$ is constant, similar R_i values would be expected for additional cycles of PGR consumption. Initial studies (Supplementary Fig. 2) showed that this is the case with the thermo-labile azo compound AAPH (100 mM), which produces peroxyl radicals at a constant rate for several hours [43], with similar R_i values obtained for the first and second cycles of PGR bleaching. However, for both SOD-1 enzymes, the initial PGR consumption rates decreased with increasing numbers of reaction cycles (Fig. 7A), consistent with time-dependent inactivation of both enzymes. When the bSOD-1 system was preincubated in the absence of PGR, and PGR then added after 10 min, kinetic profiles (Fig. 7B) compatible with those depicted in Fig. 7A were obtained. This implies that SOD-1 inactivation is not associated with the presence of PGR. Quantitatively, inactivation of both enzymes was reflected in a decrease of R_i to 60% (bSOD-1) and 75% (hSOD-1) of the initial values after 10 min, and to ~ 20% after 20 min (Supplementary Fig. 3).

As previous studies have reported oxidation of the single Trp (Trp32) of hSOD-1, by $CO_3^{\bullet-}$ generated by the peroxidase activity of the enzyme [5,10], we examined the intrinsic fluorescence of hSOD-1 (3 μM per dimer) during incubation with H_2O_2 (2 mM) in HCO_3^- buffer. The time course data (Fig. 8A) indicate a fast loss of intrinsic Trp fluorescence with an initial consumption rate of 1.3 ± 0.2 μM min^{-1}, and only 10% of the initial fluorescence intensity detected after 10 min. This decrease was inhibited by the presence of PGR (15 μM), with this inducing a lag time of ~5 min (Fig. 8A), and beyond this time point, a slower rate of fluorescence decreased than in the absence of PGR.

To compare the efficiency of bSOD-1 and hSOD-1 as oxidant source (i.e. their ability to generate $CO_3^{\bullet-}$), the consumption of free Trp (6 μM)

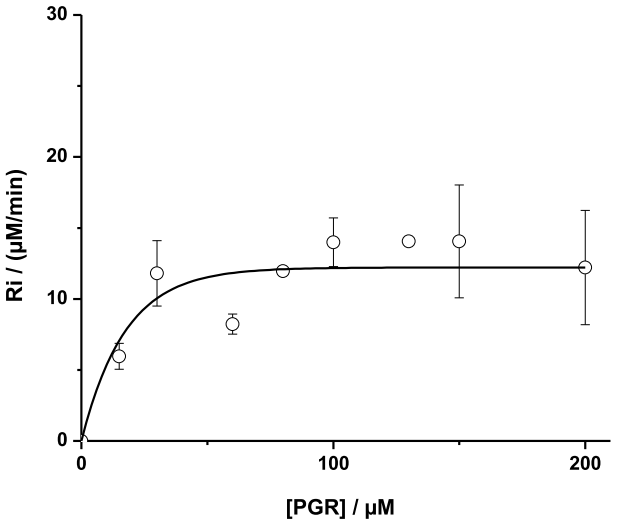

Fig. 6. Dependence on rate of PGR consumption rate (Ri) with initial PGR concentration. Solutions of PGR (15–200 μM) in bicarbonate buffer (200 mM, pH 7.4) and DTPA (0.1 mM) were incubated in the presence of bSOD-1 (3 μM) and H_2O_2 (2 mM). R_i values were determined as described in Material and Methods section.

mediated by the complete bSOD-1 system was examined. Fig. 8B shows the time course of free Trp fluorescence loss in the absence and presence of 15 μM PGR. In the absence of PGR the initial consumption rate was 2.7 ± 0.1 μM min^{-1}, and complete consumption was observed after 4 min. In the presence of PGR, similar behavior was observed to that described above for hSOD-1 (Fig. 8A), consistent with competitive oxidation of Trp and PGR by $CO_3^{\cdot -}$, with PGR being the more sensitive target.

4. Discussion

The peroxidase activity of SOD-1 has been the subject of considerable research, as under conditions of high H_2O_2 and HCO_3^- levels, oxidative effects associated with the formation of $CO_3^{\cdot -}$ have been reported [5,8,13,14,31]. In particular, $CO_3^{\cdot -}$mediated self-oxidation of bSOD-1 and hSOD-1 can occur, with this resulting in conversion of the (single) Trp32 residue in the human isoform, to tryptophan-derived indolyl radicals and inter-molecular covalent Trp-Trp bonds [10]. Thus, contrary to the traditional role of SOD-1 as an antioxidant (protective) enzyme, the production of $CO_3^{\cdot -}$ indicates that under certain circumstances this enzyme can be a source of highly-reactive and damaging oxidants. The $CO_3^{\cdot -}$ formed can react not only with readily oxidized residues in the generating protein (His, Trp and Tyr residues of bSOD-1 or hSOD-1), but also is able to damage other biological targets such as proteins and peptides [12–14,44]. These processes, together with the reaction of peroxynitrite with CO_2/HCO_3^- which results in the generation of peroxynitrosocarbonate and subsequently $CO_3^{\cdot -}$ from homolysis of this adduct [3], and potential formation by Fenton chemistry in HCO_3^- buffers [18], have positioned $CO_3^{\cdot -}$ as a relevant oxidant in biological milieu.

Formation of $CO_3^{\cdot -}$ by the peroxidase activity of SOD-1 has been demonstrated by EPR employing DMPO as the spin trap [4,14,33]. These data have been confirmed here, with the detection of DMPO-OH spin adduct arising from reaction of $CO_3^{\cdot -}$ with DMPO (k 2.5 × 10^6 $M^{-1}s^{-1}$ [33]) and subsequent hydroxylation [4,33] (Fig. 1). Quantification of $CO_3^{\cdot -}$ using this method has however been shown in this study to be compromised by the instability of the DMPO-OH spin adduct [14], with the rate of decay being dependent on the SOD concentration and further reactions, potentially resulting in an underestimation of the $CO_3^{\cdot -}$ concentration. The relationship between instability of DMPO-OH and bSOD-1 concentration could be related to disproportionation of

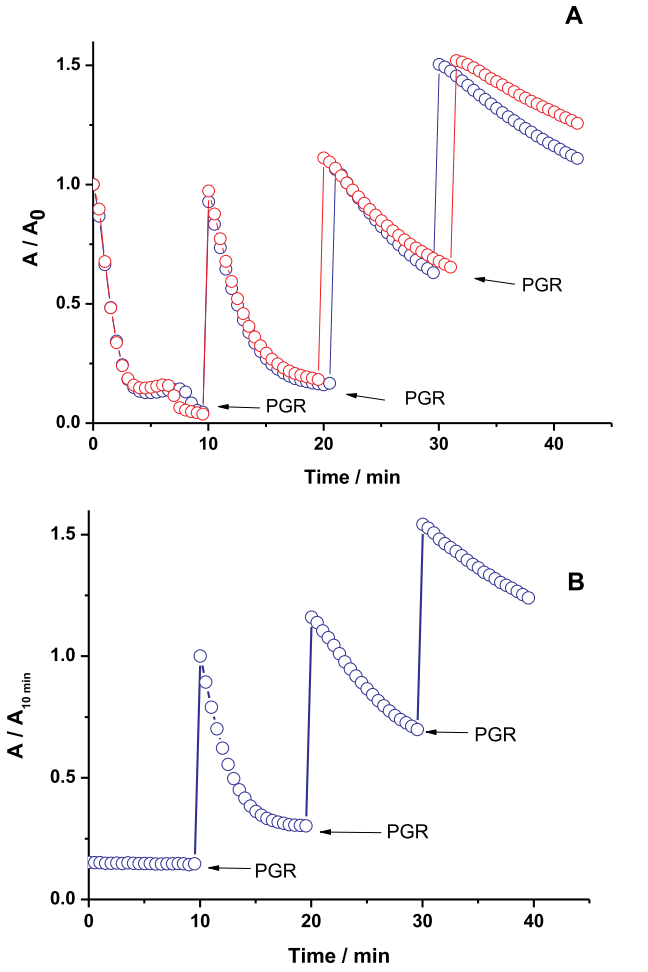

Fig. 7. Kinetic profiles of consecutive PGR oxidation cycles. Panel A: Solutions of PGR (30 μM) were incubated with bSOD-1 (blue circles) or hSOD-1 (red circles), 3 μM, H_2O_2 (2 mM) in bicarbonate buffer (200 mM, pH 7.4) containing DTPA (0.1 mM). Absorbance intensity changes were followed at 570 nm. After PGR consumption, further aliquots (30 μL) of PGR (1 mM) were added as indicated by arrows. Panel B: reaction system as in panel A, but the bSOD-1/H_2O_2 system was first pre-incubated in the absence of PGR. After 10 min incubation, aliquots (30 μL) of PGR (1 mM) were added as indicated by arrows. Representative data from n = 3 independent experiments.

DMPO-OH spin adduct which depends on the square of the $CO_3^{\cdot -}$ concentration [45].

The formation of $CO_3^{\cdot -}$ by the bSOD-1/H_2O_2/DTPA/HCO_3^- system has also been examined here, and previously [5], using ABTS as oxidizable target. ABTS oxidation produces $ABTS^{\cdot +}$, a well-known stable and colored free radical [46]. Formation of $ABTS^{\cdot +}$ has been employed to detect $CO_3^{\cdot -}$ [5] as well as other oxidants (e.g., $NO_2^{\cdot}$ [47]). In contrast, bleaching of $ABTS^{\cdot +}$ has widely used to assess antioxidant capacity of natural and synthetic compounds [46]. The EPR data obtained here showed the formation of $ABTS^{\cdot +}$ by the bSOD-1 system, but the resulting EPR spectrum was of low intensity (Fig. 2A); the identity of the observed signal was confirmed by independent generation of $ABTS^{\cdot +}$ using MnO_2 [41]. Spectrophotometric analysis of ABTS $^{\cdot +}$ formation from ABTS at 740 nm by the bSOD-1/H_2O_2/DTPA/HCO_3^- system, showed that $ABTS^{\cdot +}$ was generated efficiently with a maximum absorbance intensity detected after 9 min using 3 μM bSOD-1 and 2 mM H_2O_2 in HCO_3^- buffer. However, the absorbance from ABTS $^{\cdot +}$ was not stable over time, with the intensity decreasing by 70% with increasing incubation time (Fig. 2C). This probably reflects secondary reactions between $ABTS^{\cdot +}$ and $CO_3^{\cdot -}$ which, under conditions of H_2O_2 excess, generate over-oxidation products in a similar manner to that

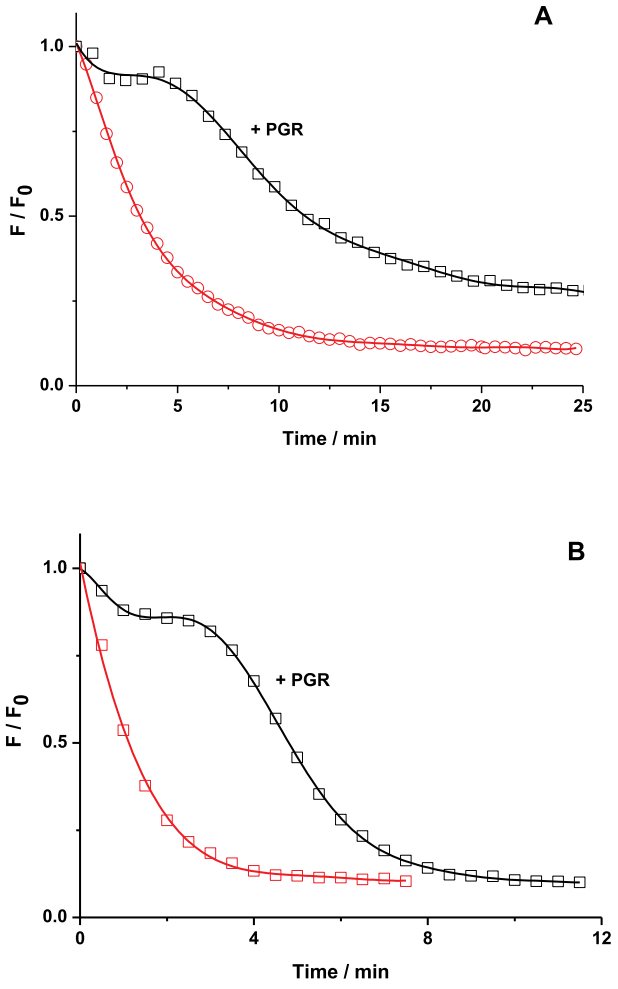

Fig. 8. Consumption of Trp and protection by PGR. Solutions containing bSOD-1 or hSOD-1 (3 μM as dimer), H_2O_2 (2 mM) and DTPA (0.1 mM) were incubated in bicarbonate buffer (200 mM, pH 7.4). Trp consumption was followed by fluorescence as described in the Materials and Methods section. Panel A: Consumption of the single Trp residue of hSOD-1 (Trp^{32}) in the absence of PGR (red circles) and in the presence of PGR (15 μM, black squares). Panel B: Consumption of free Trp (6 μM) induced by bSOD-1/H_2O_2 system in the absence of PGR (red squares) and presence of PGR (15 μM, black squares). Representative data from n = 3 independent experiments.

reported for encapsulated horseradish peroxidase [48].

Altogether these data indicate that both EPR spin trapping, and the used of ABTS (with either EPR or spectrophotometric detection) have limited use for quantifying $CO_3^{\bullet -}$ formation. These approaches are, however, valuable qualitative tools for examining $CO_3^{\bullet -}$ formation under the experimental conditions employed.

PGR has been employed previously as a probe to determine the antioxidant capacity of pure polyphenols and complex mixtures against a variety of reactive species, including $NO_2^{\bullet}$, HOCl, $RO_2^{\bullet}$, and $O_2^{\bullet -}$ [37]. The kinetics of these reactions are usually followed by the bleaching of the optical absorption band centered at 540 nm (at pH 7.4) [36–38,49]. The loss of this absorbance is accompanied by formation of a new band at 395 nm with a well-defined isosbestic point at ~440 nm, as evidenced in the first minutes of reaction [49]. This behavior is reported to relate to a two-electron process (i.e. one mol of PGR is oxidized by 2 mol of the reactive species) generating a quinone derivative [37].

PGR is bleached to only a very minor extent by H_2O_2 at concentrations < 3 mM, and that PGR does not bind strongly to bSOD-1 or hSOD-1, as evidenced by minimal changes to the shape and intensity of the UV–visible spectrum of PGR in the presence versus absence of the enzymes (data not shown). However, in the presence of bSOD-1 and H_2O_2, a fast bleaching of PGR was detected in HCO_3^- (but not phosphate) buffer in the presence of DTPA 0.1 mM (Fig. 3, and Supplementary Fig. 1). Consistent with PGR oxidation by $CO_3^{\bullet -}$. The minimal reactions involved in this process can be represented by reactions (2) and (3).

$$\text{SOD-1} \xrightarrow{H_2O_2 / HCO_3^-} CO_3^{\bullet -} \quad (2)$$

$$\text{PGR} + CO_3^{\bullet -} \longrightarrow \text{bleaching} \quad (3)$$

At low PGR concentrations not all the $CO_3^{\bullet -}$ appears to react with PGR, but secondary reactions involving bSOD-1 or self-reactions of $CO_3^{\bullet -}$ also likely to occur (reactions (4) and (5) with bSOD-1_{ox} representing product(s) of bSOD-1 oxidation by $CO_3^{\bullet -}$).

$$\text{bSOD-1} + CO_3^{\bullet -} \longrightarrow \text{bSOD-1}_{ox} + HCO_3^- \quad (4)$$

$$CO_3^{\bullet -} + CO_3^{\bullet -} \longrightarrow CO_2 + CO_4^{2-} \quad (5)$$

At high PGR concentrations all the $CO_3^{\bullet -}$ appear to react with the added probe (i.e. reactions (4) and (5) are minimal), as the rate of PGR consumption has been shown to be independent of its initial concentration, and directly proportional to the rate of $CO_3^{\bullet -}$ formation. The kinetic data presented in Fig. 5 have allowed the initial rates of consumption of PGR (R_i) to be determined. At the lowest bSOD-1 concentration studied (0.3 μM per dimer), R_i was independent of the initial PGR concentration, but at higher levels of bSOD-1 (3 μM), R_i increased for PGR concentrations between 5 and 30 μM. However, with high PGR levels (> 30 μM), R_i was independent of the initial PGR concentrations, implying that all $CO_3^{\bullet -}$ were removed by PGR (zero order kinetic limit in PGR). Under these conditions, R_i is related to the rate of $CO_3^{\bullet -}$ release by equation (6):

$$R_{CO3^{\bullet -}} = n\, R_i \quad (6)$$

Where R_i is the initial rate of PGR bleaching, n is the stoichiometric factor (defined as the number of $CO_3^{\bullet -}$ trapped by PGR), and $R_{CO3^{\bullet -}}$ is the rate of $CO_3^{\bullet -}$ release.

Under conditions where there is an excess of H_2O_2 and HCO_3^-, $R_{CO3^{\bullet -}}$ depends on the SOD-1 concentration (Fig. 4). Considering the maxima R_i values, obtained at PGR concentrations > 30 μM (with 3 μM bSOD-1, Fig. 6), and assuming $n = 2$ [37], a rate of $CO_3^{\bullet -}$ release of 24.6 ± 4.3 μM min^{-1} with 3 μM bSOD-1 can be estimated. This value, which is in the order of kinetic data of NADPH oxidation [50], represents a specific peroxidase activity close to 0.3 ± 0.1 units/mg (defining one unit as the amount of bSOD-1, in mg, that generates 1 μM of $CO_3^{\bullet -}$ min^{-1}). The estimated rate of $CO_3^{\bullet -}$ release (24.6 ± 4.3 μM min^{-1}) means a turnover (kcat) value of 8.3 min^{-1}, which is very similar of the determined from data depicted in Fig. 4 (10 min^{-1}).

In line with the structural similarity of bSOD-1 and hSOD-1 (83% homology), and published data showing similar peroxidase activity for both enzymes [31], comparable R_i values were determined for bSOD-1 and hSOD-1; 10.9 ± 1.9 and 9.6 ± 1.0 μM min^{-1}, respectively, with 3 μM enzyme. However, the rate of formation does not appear to be stable over time as a result of reactions occurring within, or close to the active site, which lead to SOD-1 inactivation. Thus in experiments in which new aliquots of PGR were added after initial bleaching, decreasing R_i values were detected with the SOD systems for different cycles of PGR consumption (Fig. 7A). This effect was not detected when AAPH was employed as the radical source, where a constant flux of radicals is formed over several hours of incubation [43]. This decrease in R_i, which is believed to reflect inactivation of SOD-1, was not related to the presence PGR, as the addition of PGR to preincubated solutions of bSOD-1 gave the same pattern of decreasing R_i values (Fig. 7B). The same behavior was observed for both bSOD-1 and hSOD-1 (Supplementary Fig. 3), with R_i values reaching close to 6.8 and 2.0 μM min^{-1} detected after 10 and 20 min incubation, respectively. This represents a decrease in the peroxidase activity of 38 and 24% after 10 min incubation for bSOD-1 and hSOD-1, respectively, and close to 80%

after 20 min. The similarity of these values suggests a common mechanism of inactivation. To explore the possible participation of the single Trp^{32} residue in hSOD-1 in inactivation, the loss of the intrinsic fluorescence arising from this amino acid was followed during incubations with H_2O_2 in HCO_3^- buffer, in the absence of PGR. The fluorescence significantly decreased over time with an initial consumption rate of 1.2 ± 0.1 μM min^{-1}, with only 17% remaining after 10 minutes (Fig. 8A). At this time point however, the peroxidase activity of hSOD-1 was 76% of the initial value (Supplementary Fig. 3), indicating that these two events are divorced from each other. This result, together with the similarity in the rates of loss of peroxidase activity of the two enzymes (Supplementary Fig. 3), and the absence of Trp^{32} from the bovine protein, suggests that oxidation of Trp^{32} of hSOD-1 does not (directly) initiate the decrease of activity, which is in line with inactivation of SOD1 due to oxidation of the histidine residues at its catalytic site [8,39]. This conclusion does not exclude the role that Trp^{32} plays in formation of Trp-Trp bonds (leading to hSOD-1 dimerization and aggregation), or the production of *N*-formylkynurenine or kynurenine on hSOD-1 oxidation [5,8,10,11,14].

Consumption of hSOD-1 Trp^{32} was compared with that for free Trp (at the same concentration, 6 μM) elicited by the peroxidase activity of bSOD-1. As presented in Fig. 8B, an efficient consumption of free Trp was observed, with an initial consumption rate (2.9 ± 0.2 μM min^{-1}) approximately 2-fold higher than for Trp^{32}. The later is in agreement with the oxidation of both Trp^{32} and free Trp induced by AAPH-derived free radicals [51]. PGR (15 μM) protected both Trp^{32} and free Trp (induced by bSOD-1) from consumption, as reflected by lag times of 3.5 and 5 min in the kinetic profiles of fluorescence decrease for Trp^{32} and free Trp, respectively (Fig. 8). From these lag times, and considering $n = 2$, $R_{CO3}\cdot^-$ values of 8.5 and 6 μM min^{-1} were estimated for both systems. These values are lower than $R_{CO3}\cdot^-$ determined from data presented in Figs. 4 and 6. Such difference can be explained by the low PGR concentrations employed in the experiments reported in Fig. 8, implicating the participation of reactions (4) and (5).

5. Conclusions

These results show that PGR reacts with the $CO_3\cdot^-$ generated from the peroxidase activity of SOD-1. At high PGR concentrations, the initial consumption rates (R_i) reflect the rate of $CO_3\cdot^-$ formation, giving a rate of 24.6 ± 4.3 μM min^{-1} with 3 μM (dimeric) SOD-1. From the kinetic data for PGR consumption, we determined a high rate of SOD-1 inactivation during the first 20 min of reaction. In the case of the human isoform this inactivation appears to be unrelated to Trp^{32} consumption. The PGR bleaching protocol described here therefore appears to be a simple, fast and inexpensive assay to determine $CO_3\cdot^-$ generation from the peroxidase activity of SOD-1 under isolated protein conditions. It should however, be noted that PGR is not selective for $CO_3\cdot^-$ which could limit the use of this probe in complex systems.

Acknowledgments

This work was supported by FONDECYT (grant n°1180642). JDF acknowledges a VRI fellowship from PUC. MJD gratefully acknowledges financial support from the Novo Nordisk Foundation (Laureate grant: NNF13OC0004294).

Appendix A. Supplementary data

Supplementary data to this article can be found online at https://doi.org/10.1016/j.redox.2019.101207.

References

[1] B. Halliwell, J.M.C. Gutteridge, 5th ed., Free Radic. Biol. Medic, (2015) United Kingdom: Oxford.
[2] S.I. Liochev, I. Fridovich, CO2 enhanced peroxidase activity of SOD1: the effects of pH, Free Radic. Biol. Med. 36 (2004) 1444–1447.
[3] O. Augusto, M.G. Bonini, A.M. Amanso, E. Linares, C.C.X. Santos, S.L. De Menezes, Nitrogen dioxide and carbonate radical anion: two emerging radicals in biology, Free Radic. Biol. Med. 32 (2002) 841–859.
[4] D.B. Medinas, G. Cerchiaro, D.F. Trindade, O. Augusto, The carbonate radical and related oxidants derived from bicarbonate buffer, IUBMB Life 59 (2007) 255–262.
[5] H. Zhang, C. Andrekopoulos, J. Joseph, J. Crow, B. Kalyanaraman, The carbonate radical anion-induced covalent aggregation of human copper, zinc superoxide dismutase, and α-synuclein: intermediacy of tryptophan- and tyrosine-derived oxidation products, Free Radic. Biol. Med. 36 (2004) 1355–1365.
[6] S. Sankarapandi, J.L. Zweier, Bicarbonate is required for the peroxidase function of Cu, Zn-superoxide dismutase at physiological pH, J. Biol. Chem. 274 (1999) 1226–1232.
[7] S.P.A. Goss, R.J. Singh, B. Kalyanaraman, Bicarbonate enhances the peroxidase activity of Cu,Zn-superoxide dismutase. Role of carbonate anion radical, J. Biol. Chem. 274 (1999) 28233–28239.
[8] D.C. Ramirez, S.E. Gomez-Mejiba, J.T. Corbett, L.J. Deterding, K.B. Tomer, R.P. Mason, Cu,Zn-superoxide dismutase-driven free radical modifications: copper- and carbonate radical anion-initiated protein radical chemistry, Biochem. J. 417 (2009) 341–353.
[9] K. Chandran, J. McCracken, F.C. Peterson, W.E. Antholine, B.F. Volkman, B. Kalyanaraman, Oxidation of histidine residues in copper−zinc superoxide dismutase by bicarbonate-stimulated peroxidase and thiol oxidase activities: pulse EPR and NMR studies, Biochemistry 49 (2010) 10616–10622.
[10] D.B. Medinas, F.C. Gozzo, L.F.A. Santos, A.H. Iglesias, O. Augusto, A ditryptophan cross-link is responsible for the covalent dimerization of human superoxide dismutase 1 during its bicarbonate-dependent peroxidase activity, Free Radic. Biol. Med. 49 (2010) 1046–1053.
[11] F.R. Coelho, A. Iqbal, E. Linares, D.F. Silva, F.S. Lima, I.M. Cuccovia, O. Augusto, Oxidation of the tryptophan 32 residue of human superoxide dismutase 1 caused by its bicarbonate-dependent peroxidase activity triggers the non-amyloid aggregation of the enzyme, J. Biol. Chem. 289 (2014) 30690–30701.
[12] L. Carroll, D.I. Pattison, J.B. Davies, R.F. Anderson, C. Lopez-Alarcon, M.J. Davies, Formation and detection of oxidant-generated tryptophan dimers in peptides and proteins, Free Radic. Biol. Med. 113 (2017) 132–142.
[13] V. Paviani, G. Galdino, J. dos Prazeres, R. Queiroz, O. Augusto, V. Paviani, G.T. Galdino, J.N. dos Prazeres, R.F. Queiroz, O. Augusto, Ditryptophan cross-links as novel products of protein oxidation, J. Braz. Chem. Soc. 29 (2017) 925–933.
[14] V. Paviani, R.F. Queiroz, E.F. Marques, P. Di Mascio, O. Augusto, Production of lysozyme and lysozyme-superoxide dismutase dimers bound by a ditryptophan cross-link in carbonate radical-treated lysozyme, Free Radic. Biol. Med. 89 (2015) 72–82.
[15] G.E. Adams, J.E. Aldrich, R.H. Bisby, R.B. Cundall, J.L. Redpath, R.L. Willson, Selective free radical reactions with proteins and enzymes: reactions of inorganic radical anions with amino acids, Radiat. Res. 49 (1972) 278–289.
[16] S. Chen, M.Z. Hoffman, Rate constants for the reaction of the carbonate radical with compounds of biochemical interest in neutral aqueous solution, Radiat. Res. 56 (1973) 40–47.
[17] A. Iqbal, V. Paviani, A.I. Moretti, F.R.M. Laurindo, O. Augusto, Oxidation, inactivation and aggregation of protein disulfide isomerase promoted by the bicarbonate-dependent peroxidase activity of human superoxide dismutase, Arch. Biochem. Biophys. 557 (2014) 72–81.
[18] E. Illés, A. Mizrahi, V. Marks, D. Meyerstein, Carbonate-radical-anions, and not hydroxyl radicals, are the products of the Fenton reaction in neutral solutions containing bicarbonate, Free Radic. Biol. Med. 131 (2019) 1–6.
[19] M.M. Zhang, D.L. Rempel, M.L. Gross, A fast photochemical oxidation of proteins (FPOP) platform for free-radical reactions: the carbonate radical anion with peptides and proteins, Free Radic. Biol. Med. 131 (2019) 126–132.
[20] C. Busset, P. Mazellier, M. Sarakha, J. De Laat, Photochemical generation of carbonate radicals and their reactivity with phenol, J. Photochem. Photobiol. A Chem. 185 (2007) 127–132.
[21] M.G. Bonini, S. Miyamoto, P. Di Mascio, O. Augusto, Production of the carbonate radical anion during xanthine oxidase turnover in the presence of bicarbonate, J. Biol. Chem. 279 (2004) 51836–51843.
[22] L. Gebicka, J. Didik, J.L. Gebicki, Reactions of heme proteins with carbonate radical anion, Res. Chem. Intermed. 35 (2009) 401–409.
[23] M. Carlsson, D. Stenman, M. Jonsson, T. Reitberger, Reactivity of the carbonate radical anion towards carbohydrate and lignin model compounds, J. Wood Chem. Technol. 23 (2003) 47–69.
[24] V. Shafirovich, A. Dourandin, W. Huang, N.E. Geacintov, The carbonate radical is a site-selective oxidizing agent of guanine in double-stranded oligonucleotides, J. Biol. Chem. 276 (2001) 24621–24626.
[25] A. Denicola, B.A. Freeman, M. Trujillo, R. Radi, Peroxynitrite reaction with carbon dioxide/bicarbonate: kinetics and influence on peroxynitrite-mediated oxidations, Arch. Biochem. Biophys. 333 (1996) 49–58.
[26] S. Goldstein, G. Czapski, Formation of peroxynitrate from the reaction of peroxynitrite with CO2: evidence for carbonate radical production, (1998), J. Am. Chem. Soc. 120 (1998) 3458–3463.
[27] R. Radi, Peroxynitrite, a stealthy biological oxidant, J. Biol. Chem. 288 (2013) 26464–26472.
[28] E.C. Kennett, M.J. Davies, Glycosaminoglycans are fragmented by hydroxyl, carbonate, and nitrogen dioxide radicals in a site-selective manner: implications for peroxynitrite-mediated damage at sites of inflammation, Free Radic. Biol. Med. 47 (2009) 389–400.
[29] H. Zhang, J. Joseph, M. Gurney, D. Becker, B. Kalyanaraman, Bicarbonate enhances

peroxidase activity of Cu,Zn-superoxide dismutase. Role of carbonate anion radical and scavenging of carbonate anion radical by metalloporphyrin antioxidant enzyme mimetics, J. Biol. Chem. 277 (2002) 1013–1020.
[30] P. Wardman, Fluorescent and luminescent probes for measurement of oxidative and nitrosative species in cells and tissues: progress, pitfalls, and prospects, Free Radic. Biol. Med. 43 (2007) 995–1022.
[31] R.F. Queiroz, V. Paviani, F.R. Coelho, E.F. Marques, P. Di Mascio, O. Augusto, The carbonylation and covalent dimerization of human superoxide dismutase 1 caused by its bicarbonate-dependent peroxidase activity is inhibited by the radical scavenger tempol, Biochem. J. 455 (2013) 37–46.
[32] A. Baseggio Conrado, S. Maina, H. Moseley, A. Francioso, L. Mosca, E. Capuozzo, M. Fontana, Carbonate anion radical generated by the peroxidase activity of copper-zinc superoxide dismutase: scavenging of radical and protection of enzyme by hypotaurine and cysteine sulfinic acid, in: D.H. Lee, S.W. Schaffer, E. Park, H.W. Kim (Eds.), Taurine 10. Advances in Experimental Medicine and Biology, vol. 975, Springer, Dordrecht, 2017.
[33] M.N. Alvarez, G. Peluffo, L. Folkes, P. Wardman, R. Radi, Reaction of the carbonate radical with the spin-trap 5,5-dimethyl-1-pyrroline-N-oxide in chemical and cellular systems: pulse radiolysis, electron paramagnetic resonance, and kinetic-competition studies, Free Radic. Biol. Med. 43 (2007) 1523–1533.
[34] M. Takashima, M. Horie, M. Shichiri, Y. Hagihara, Y. Yoshida, E. Niki, Assessment of antioxidant capacity for scavenging free radicals in vitro: a rational basis and practical application, Free Radic. Biol. Med. 52 (2012) 1242–1252.
[35] J. Cortés-Ríos, M.J. Torres, M.P. Campos-Bustamante, J. Romero-Parra, M.E. Letelier, D. Pessoa-Mahana, H. Chung, M. Faúndez, NADPH oxidase activity: spectrophotometric determination of superoxide using pyrogallol red, Anal. Biochem. 536 (2017) 96–100.
[36] M. Faúndez, M. Rojas, P. Bohle, C. Reyes, M.E. Letelier, M.E. Aliaga, H. Speisky, E. Lissi, C. López-Alarcón, Pyrogallol red oxidation induced by superoxide radicals: application to evaluate redox cycling of nitro compounds, Anal. Biochem. 419 (2011) 284–291.
[37] E. Atala, G. Velásquez, C. Vergara, C. Mardones, J. Reyes, R.A. Tapia, F. Quina, M.A. Mendes, H. Speisky, E. Lissi, M.S. Ureta-Zañartu, A. Aspée, C. López-Alarcón, Mechanism of pyrogallol red oxidation induced by free radicals and reactive oxidant species. A kinetic and spectroelectrochemistry study, J. Phys. Chem. B 117 (2013) 4870–4879.
[38] C. López-Alarcón, E. Lissi, A novel and simple ORAC methodology based on the interaction of pyrogallol red with peroxyl radicals, Free Radic. Res. 40 (2006) 979–985.
[39] B. Alvarez, V. Demicheli, R. Durán, M. Trujillo, C. Cerveñansky, B.A. Freeman, R. Radi, Inactivation of human Cu,Zn superoxide dismutase by peroxynitrite and formation of histidinyl radical, Free Radic. Biol. Med. 37 (2004) 813–822.
[40] J.M. Fontmorin, R.C. Burgos Castillo, W.Z. Tang, M. Sillanpää, Stability of 5,5-dimethyl-1-pyrroline- N -oxide as a spin-trap for quantification of hydroxyl radicals in processes based on Fenton reaction, Water Res. 99 (2016) 24–32.
[41] C. Henriquez, C. Aliaga, E. Lissi, Formation and decay of the ABTS derived radical cation: a comparison of different preparation procedures, Int. J. Chem. Kinet. 34 (2002) 659–665.
[42] B.S. Wolfenden, R.L. Willson, Radical-cations as reference chromogens in kinetic studies of ono-electron transfer reactions: pulse radiolysis studies of 2,2′-azinobis-(3-ethylbenzthiazoline-6-sulphonate), J. Chem. Soc. Perkin Trans. 2 (0) (1982) 805–812.
[43] E. Niki, Free radical initiators as source of water- or lipid-soluble peroxyl radicals, Methods Enzymol. 186 (1990) 100–108.
[44] D.C. Ramirez, S.E. Gomez Mejiba, R.P. Mason, Mechanism of hydrogen peroxide-induced Cu,Zn-superoxide dismutase-centered radical formation as explored by immuno-spin trapping: the role of copper- and carbonate radical anion-mediated oxidations, Free Radic. Biol. Med. 38 (2005) 201–214.
[45] Y. Kirino, T. Ohkuma, T. Kwan, Spin trapping with 5, 5-dimethylpyrroline-N-oxide in aqueous solution, Chem. Pharm. Bull. 29 (1981) 29–34.
[46] R. Re, N. Pellegrini, A. Proteggente, A. Pannala, M. Yang, C. Rice-Evans, Antioxidant activity applying an improved ABTS radical cation decolorization assay, Free Radic. Biol. Med. 26 (1999) 1231–1237.
[47] A.A. Salem, A.A. Soliman, I.A. El-Haty, New spectrophotometric method for determining nitrogen dioxide in air using 2,2-azino-bis(3-ethyl benzothiazoline)-6-sulfonic acid-diammonium salt and passive sampling, Anal. Chem. Insights 6 (2011) 37–44.
[48] E.N. Kadnikova, N.M. Kostic, Oxidation of ABTS by hydrogen peroxide catalyzed by horseradish peroxidase encapsulated into sol–gel glass. Effects of glass matrix on reactivity, J. Mol. Catal. B Enzym. 18 (2002) 39–48.
[49] C. López-Alarcón, E. Lissi, Interaction of pyrogallol red with peroxyl radicals. A basis for a simple methodology for the evaluation of antioxidant capabilities, Free Radic. Res. 39 (2005) 729–736.
[50] S.I. Liochev, I. Fridovich, Copper, zinc superoxide dismutase and H2O2. Effects of bicarbonate on inactivation and oxidations of NADPH and urate, and on consumption of H2O2, J. Biol. Chem. 277 (2002) 34674–34678.
[51] E. Fuentes-Lemus, E. Dorta, E. Escobar, A. Aspée, E. Pino, M.L. Abasq, H. Speisky, E. Silva, E. Lissi, M.J. Davies, C. López-Alarcón, Oxidation of free, peptide and protein tryptophan residues mediated by AAPH-derived free radicals: role of alkoxyl and peroxyl radicals, RSC Adv. 6 (2016) 57948–57955.